



# Arctic ice clouds over northern Sweden: microphysical properties studied with the Balloon-borne Ice Cloud particle Imager B-ICI

Veronika Wolf<sup>1</sup>, Thomas Kuhn<sup>1</sup>, Mathias Milz<sup>1</sup>, Peter Voelger<sup>2</sup>, Martina Krämer<sup>3</sup>, and Christian Rolf<sup>3</sup>

<sup>1</sup>Luleå University of Technology, Division of Space Technology, Kiruna, Sweden

<sup>2</sup>Swedish Institute of Space Physics (IRF), Solar Terrestrial and Atmospheric Research Programme, Kiruna, Sweden

<sup>3</sup>Research Centre Jülich, Institute for Energy and Climate Research 7: Stratosphere (IEK-7), Jülich, Germany

**Correspondence:** Veronika Wolf (veronika.wolf@ltu.se)

Received: 14 April 2018 – Discussion started: 2 May 2018

Revised: 1 November 2018 – Accepted: 3 November 2018 – Published: 7 December 2018

**Abstract.** Ice particle and cloud properties such as particle size, particle shape and number concentration influence the net radiation effect of cirrus clouds. Measurements of these features are of great interest for the improvement of weather and climate models, especially for the Arctic region. In this study, balloon-borne in situ measurements of Arctic cirrus clouds have been analysed for the first time with respect to their origin. Eight cirrus cloud measurements have been carried out in Kiruna (68° N), Sweden, using the Balloon-borne Ice Cloud particle Imager (B-ICI). Ice particle diameters between 10 and 1200 µm have been found and the shape could be recognized from 20 µm upwards. Great variability in particle size and shape is observed. This cannot simply be explained by local environmental conditions. However, if sorted by cirrus origin, wind and weather conditions, the observed differences can be assessed. Number concentrations between 3 and 400 L<sup>-1</sup> have been measured, but the number concentration has reached values above 100 L<sup>-1</sup> only for two cases. These two cirrus clouds are of in situ origin and have been associated with waves. For all other measurements, the maximum ice particle concentration is below 50 L<sup>-1</sup> and for one in situ origin cirrus case only 3 L<sup>-1</sup>. In the case of in situ origin clouds, the particles are all smaller than 350 µm diameter. The PSDs for liquid origin clouds are much broader with particle sizes between 10 and 1200 µm. Furthermore, it is striking that in the case of in situ origin clouds almost all particles are compact (61 %) or irregular (25 %) when examining the particle shape. In liquid origin clouds, on the other hand, most particles are irregular (48 %), rosettes (25 %) or columnar (14 %). There are hardly any plates in cirrus re-

gardless of their origin. It is also noticeable that in the case of liquid origin clouds the rosettes and columnar particles are almost all hollow.

## 1 Introduction

Cirrus clouds have a great influence on the radiation balance of the Earth and thus also on the climate (Liou, 1986; Sassen and Comstock, 2001). However, despite decades of research there are still questions which are not fully answered (Potter and Cess, 2004; Boucher et al., 2013). Some open questions are, for example, the following. How are the ice particles distributed vertically? How many small particles (< 50 µm) are contained in a cloud and contribute to the ice water content (IWC) and optical properties? What are the optical properties of complex ice particle shapes? Imprecise knowledge of ice particle and cloud properties, such as particle size, shape and number concentration, leads to a remaining uncertainty about the radiation effect of the clouds and the resulting impact on the climate. Depending on various particle and cloud properties, cirrus clouds can have a warming or also a cooling effect (Freeman and Liou, 1979; Liou, 1986; Platt, 1989; Kienast-Sjögren et al., 2016).

Particle shape and size distribution information are important for a more precise parameterization in models to better calculate the radiant fluxes, as described by Schlimme et al. (2005). A result of their study was that particle shape has a greater influence on the optical properties of the cloud than size distribution. In addition to shape and size distribution,

roughness and hollowness of the particles are also of interest, as they also influence the optical properties, as described for example by Tang et al. (2017). Gu et al. (2011) confirmed that accurate knowledge of particle properties leads to better and more realistic parameterizations and can thus improve the retrievals for remote sensing methods as well as weather and climate models.

Several studies (e.g. Lynch, 2002; Spichtinger et al., 2005; Krämer et al., 2016; Heymsfield et al., 2017, and references therein) have shown how ice cloud properties depend on meteorological and ambient conditions, such as frontal systems, waves, temperature and humidity. Spichtinger et al. (2005), for example, described that uplift by waves not only led to an increase in supersaturation, but also to the formation of a cirrus that became optically thick within 2 hours. Also, Krämer et al. (2016) found different cirrus types, which are dependent on the formation mechanism and can be thicker (more IWC) or thinner (less IWC) due to the speed of the up-draught. They have found that a cirrus with high (low) IWC is associated with a high (low) particle concentration.

In addition to considering the local environmental conditions, ice clouds may be classified and analysed with respect to conditions at their origin (Krämer et al., 2016; Wernli et al., 2016). Certain characteristic properties may then be attributed to one of two origin types, liquid origin or in situ origin.

The Fourth Assessment Report of the Intergovernmental Panel on Climate Change (Solomon et al., 2007) points out that improved knowledge about clouds in the Arctic is a priority because the high latitudes are much more affected by climate change than other latitudes. Due to the remoteness of large parts of the Arctic region, clouds there have been studied far less often than at other latitudes. Furthermore, most of the measuring campaigns in the Arctic have been aircraft measurements but not always especially dedicated to Arctic cirrus measurements. Campaigns in which cirrus clouds were investigated are, for example, POLSTAR 1997 (Schiller et al., 1999), FIRE-ACE 1998 (Lawson et al., 2001), INTACC 1999 (Field et al., 2001), ASTAR 2004 (Gayet et al., 2007), M-PACE 2004 (Verlinde et al., 2007) and ISDAC 2008 (McFarquhar et al., 2011).

Ice particle sampling by aircraft suffered from shattering effects at the instrument inlet due to high aircraft speed (e.g. Korolev et al., 2011, 2013; Jackson et al., 2014). This shattering led to incorrect size distributions with too many small particles. A new inlet design and algorithm might overcome this problem, at least partly (Korolev et al., 2013; Jackson et al., 2014). Another problem with aircraft measurements, where the instrument is fixed under the wing, is that the air around the wing is compressed and in order to calculate the number concentration, the temperature and pressure must be corrected to match the ambient undisturbed conditions (Weigel et al., 2016). Balloon-borne measurements avoid both of these issues. An additional advantage of balloon-borne measurements is that vertical cloud profiles can be

measured with high spatial resolution. Furthermore, it is possible to measure with very high image resolution.

This study discusses balloon-borne measurements of particle properties with a particular emphasis on particle shape and size. For this, particles were imaged with a very high image resolution (1 pixel = 1.65  $\mu\text{m}$ ) so that the shape is identifiable from a size of 20  $\mu\text{m}$  upwards. For aircraft measurements, in comparison, the often used optical array probes record the shadow of particles with pixel resolutions between 10 and 25  $\mu\text{m}$  (Knollenberg, 1981; Lawson et al., 2006; Baumgardner et al., 2017). The cloud particle imager (CPI; Lawson et al., 2001) has a comparable pixel resolution of 2.3  $\mu\text{m}$  so that it may be used for smaller particles if they are in focus.

The balloon-borne in situ measurements have been carried out north of the Arctic Circle in Kiruna, in order to obtain high-resolution images of ice particles in cirrus clouds and thus provide accurate information on Arctic cirrus clouds and their particles. The measured cirrus clouds have been sorted according to their cloud origin, the meteorological situation and the wind direction. The analysis focuses on ice particle shape, size and number concentration in relation to these conditions. The following sections describe the measurements and the instruments used. The collected data are then presented, analysed and discussed. Finally, the results are summarized.

## 2 Campaign description

### 2.1 Location and general meteorological conditions

Balloon-borne in situ cirrus measurements have been carried out at Esrange Space Center (ESRANGE), which is a rocket range and research centre 40 km east of Kiruna. Kiruna (68° N, 20° E) has a subarctic climate as it is located north of the Arctic Circle and east of the Scandinavian Mountains.

During winter months the conditions are influenced by the Arctic polar vortex, which is highly variable on the Northern Hemisphere. Kiruna is often close to the edge or inside the polar vortex with low temperatures in the lower and middle stratosphere. However, the weather as well as the polar vortex is also influenced by the positions of the planetary Rossby waves that determine the mid- and high-latitude weather. In early winter, but even later, the weather situation is usually still very unstable with a stronger influence of the low-pressure systems along the polar front, leading to wind mostly from the westerly directions, over the mountain range, but even from the south-east pushing air masses from the Baltic Sea over the north of Sweden. Under stable conditions, that usually occur later in winter, with Kiruna being close to or inside the polar vortex, winds from westerly directions prevail and lead the air masses over the Scandinavian mountain range. Over Kiruna and ESRANGE the

increased chance for orographically induced waves leads to observations of related cloud formations. Additionally, under stable winter conditions, e.g. due to the influence of the Arctic and Siberian high pressure, the low amount of sunlight leads to a continuous radiative cooling that causes low temperatures in the lower and middle troposphere. This leads to very strong ground inversions, and approaching frontal systems often dissolve.

All measurement days are in the winter season between the end of November and the beginning of April. Above ESRANGE the minimum temperature in the troposphere during the measurement days is between  $-70$  and  $-55$  °C. Meteorological conditions on these days are described in Sect. 3.1.

## 2.2 Measurement methods

For balloon-borne measurements of cloud and ice particle properties, an in situ imager, the Balloon-borne Ice Cloud particle Imager (B-ICI), and a radiosonde have been used. For a typical measurement, both are carried by the same balloon, ascending at an average vertical speed of approximately  $4\text{ m s}^{-1}$  through the troposphere and up to an altitude of about 13 km. The balloon type used is a plastic balloon (Raven Aerostar,  $500\text{ m}^3$ ). Auxiliary data from two lidars, one located at the Swedish Institute of Space Physics (IRF, Kiruna) and one at ESRANGE, as well as a radar located at ESRANGE are also used. The heart of these measurements is the in situ imager. This device with related methods and the instruments to support the measurements are described in this section.

### 2.2.1 In situ imager

The in situ imager, B-ICI, was built for this campaign and is a light-weight (approx. 3 kg) probe for balloon-borne use. In an experiment, while ascending through the vertical extent of encountered ice clouds, it captures ice cloud particles and images them optically with a high-resolution CCD camera. The images are stored on a memory card for post-flight analysis. Then, at a height of about 13 km, the instrument is cut off from the balloon and descends with a parachute back to ground, where it can be recovered. All measurements reported here have been carried out during winter months when ground was covered by snow and lakes were frozen. This allowed for safe landings and subsequent easy recovery of the instrument payload and image data by helicopter.

The balloon-borne probe B-ICI has been described by Kuhn et al. (2013) and Kuhn and Heymsfield (2016); however, for clarity, details of the instrument will be provided here too. Figure 1 shows the top view of the instrument with removed covers. It consists of two main units: the ice particle collecting and imaging unit which comprises the inlet (label a in Fig. 1), oil-coated film (b) and part of the imaging optics (microscope objective, mirror and illuminating LED); and the control unit comprising battery, camera (c), motor (d)

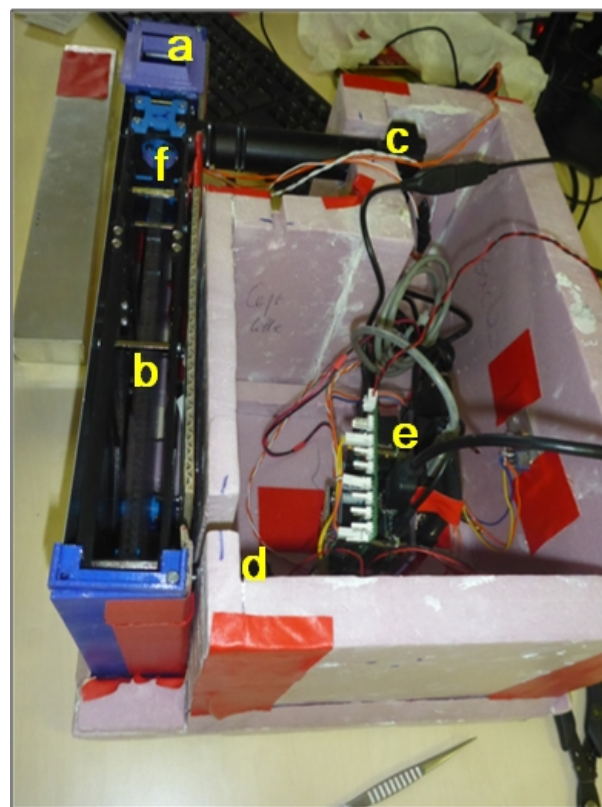


**Figure 1.** Top view on the open in situ imager B-ICI. (a) Inlet where particles enter during measurement; (b) oil-coated moving film; (c) CCD camera with an objective takes grey-map pictures every 1 s; (d) motor which moves the film; (e) computer and battery; (f) LED to illuminate the film.

and computer (e). As the imager is ascending under the balloon, ice particles enter through the inlet. The inlet opening is approximately  $31\text{ mm} \times 31\text{ mm}$ , so that at any moment a 31 mm long section of the oil-coated film is exposed to cloud ice particles. The 4 m long film is continuously moving at constant speed ( $1.1\text{ mm s}^{-1}$ ) to always expose new, un-used film and avoid superposition of particles. The film is 8 mm wide and centred under the inlet so that air will pass around the film on either side. Directly beneath the inlet, an opening on the lower side of the instrument's collecting unit with the same dimensions as the inlet allows air to move through the collecting unit. Ice particles entering directly above the film, due to their inertia, do not follow this air stream around the film and collide with it instead. Thus, these ice particles are collected, and due to the oil-coating will stay on the film. The collection efficiency has been discussed by Kuhn and Heymsfield (2016) and is 50 % at approximately  $12\text{ }\mu\text{m}$  and 80 % at around  $25\text{ }\mu\text{m}$  and higher for larger particles.

A camera system images the film 38 mm from the inlet. Hence, ice particles on the film are photographed shortly after collection. This camera system consists of a microscope objective, a tube lens and a CCD sensor ( $1280 \times 960$  pix-

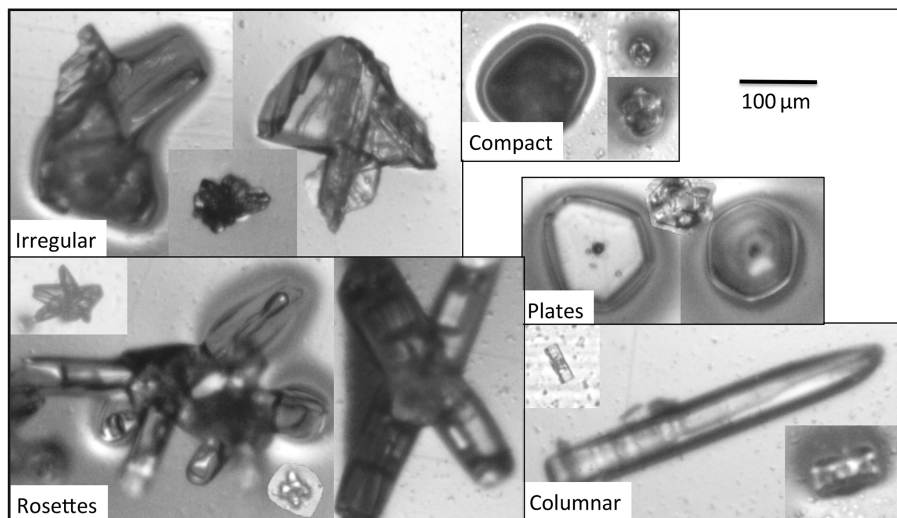


**Figure 2.** Classification of the different particles into five shape groups: compact, irregular, columnar, plates and rosettes.

els). The imaging optics has a high pixel resolution of  $1.65 \mu\text{m pixel}^{-1}$  and an optical resolution of approximately  $4 \mu\text{m}$  (as judged from the smallest details that can be discerned on the images).

### 2.2.2 Image processing

After recovery of the instrument and its image data, images are retrieved from the memory card for the following image processing on an office computer. In the first step of the three-step image processing procedure, particles are traced manually aided by a graphical computer program. This step could not be automated yet due to effects of the oil coating creating both shadows and bright regions around ice particles. In the second step, these outlines are filled and images are converted to binary masks with *true* pixels representing ice particles (belonging to one of the filled outlines) and *false* pixels representing background pixels not belonging to any filled outline. Ice particles on the binary masks are identified and their edges are found (with the MATLAB function `bwboundaries`). Then, particle size, area, area ratio and number concentration are determined from these particle edges. This second step is carried out automatically.

As a measure of particle size, we use a particle maximum dimension,  $D_{\text{max}}$ . Several different definitions of particle maximum dimension are in use in the literature (see for example Wu and McFarquhar, 2016, and references therein) and we have chosen the diameter of the smallest circle that encloses the whole particle. The number concentration  $n$  is determined from the number of ice particles collected on a given area of the film. The conversion accounts for the instrument's sample flow rate of approximately  $130 \text{ cm}^3 \text{ s}^{-1}$  and has been described by Kuhn and Heymsfield (2016). Particle size distributions  $dn/dD_{\text{max}} = N$  are then derived from  $n$  in size bins (equally spaced on a linear size scale) by divid-

ing  $n$  by the size bin width. It should be noted here that the sampling flow rate of the B-ICI, and also the sample volume, is independent of the particle size for sizes above approximately  $25 \mu\text{m}$ , where sampling efficiency approaches 100 % (see above). For most aircraft-mounted probes such as the optical array probes this is not the case and sample volume directly depends on particle size, in particular for particles below about  $200 \mu\text{m}$  in size, which results in large uncertainties in the sample volume depending on the choice of particle maximum dimension (Wu and McFarquhar, 2016). Our choice of maximum dimension is the one recommended by Wu and McFarquhar (2016), and, due to the size-independent sample volume here, it does not have an important impact on the derived number concentrations and size distributions.

In the third step, ice particles are manually classified into shapes by looking at each individual ice particle. The high-resolution images of ice particles allow us to identify shapes of particles with sizes of approximately  $20 \mu\text{m}$  (12 pixels) or larger. Each ice particle is assigned to one of five shape groups: *compact*, *irregular*, *rosettes*, *plates* or *columnar* particles. These groups were defined based on a classification by Bailey and Hallett (2009). Figure 2 shows cases of each group. Compact particles have no pronounced features deviating from a compact geometry and include particles of spheroidal shape. Rosettes include all types of bullet rosettes, column rosettes, sheath rosettes and irregular rosettes. Rosettes can have two or more arms. Plates and columnar particles are symmetrical with simple hexagonal geometries. They will most likely attach to the oil-coated film with one of their facets having the longest dimension. Thus, we classify particles visible with a hexagonal basal facet as plates and ice particles that show the longer prism facets as columnar. In addition to hexagonal columns, the shape group of columnar particles also includes single bullets. Irregulars

**Table 1.** List of measurement days, launch and cut-off times, cloud height, mean temperature, cloud origins, and meteorological situations.

Date	Flight time start – cut off UTC	Cloud height base – top m	<i>T</i> °C	Origin	Meteorological situation	wind direction	waves
4 Apr 2012	12:09 – 13:08	5550 – 7270	−49.5	in situ	occlusion	NW	waves
20 Feb 2013	11:15 – 12:17	8980 – 10 440	−62.3	in situ	orographic/before cold front	NW	waves
15 Mar 2016	08:26 – 09:38	8950 – 11 550	−56.5	in situ	orographic/before cold front	NW	waves
15 Dec 2016	10:03 – 11:04	10 120 – 11 750	−65.5	in situ	occlusion	NW	no waves
18 Dec 2013	10:45 – 11:46	7960 – 8050	−52.6	liquid	occlusion	NW	waves
20 Mar 2014	12:39 – 13:42	6020 – 8630	−49.3	liquid	warm front	NW	no waves
1 Apr 2015	09:40 – 10:34	1940 – 8410	−34.2	liquid	low-pressure centre/after occlusion	SSW	no waves
12 Feb 2016	09:38 – 10:42	3400 – 10 640	−38.7	liquid	warm front	SSW	no waves

are those particles that cannot be sorted into any other group. For each measured cirrus cloud, all particles are assigned to one of the five shape groups.

The vertical resolution of particle number concentrations and size distributions depend on the number (or number concentration) of collected particles. In the case of high particle number concentration, averaging over 10 s is sufficient, which corresponds to around 40 m vertically. For the size distributions, a slightly higher averaging period has to be used. If the particle number concentration is low, only one size distribution over the whole cloud can be averaged. This results in different vertical resolutions for the different measurement flights.

The sizing accuracy can be estimated by assuming an effective error of a few pixels when tracing the outline of ice particles. For small particles with about 20 µm (12 pixels) in size this error may be estimated as 2 pixels corresponding to approximately 17 % sizing error. For larger ice particles the error can be of the order of 3 pixels or 5 µm, which corresponds to 10 % for a 50 µm ice particle and 5 % and less for 100 µm or larger ice particles. This is similar to the experimentally determined sizing error of 4 % by Kuhn et al. (2012) who used comparable imaging optics.

### 2.2.3 Radiosonde, lidars and radar

A radiosonde is connected to the in situ imager B-ICI. It measures temperature, humidity, altitude and geographical position. Thus, these parameters can be assigned to the photographed ice particles. The RS92 from Vaisala is used for these measurements.

If available, the data from simultaneous observations by a radar and two lidars located in Kiruna and surrounding are also used. ESRAD, an atmospheric mesosphere–stratosphere–troposphere radar (Kirkwood et al., 2007) located at ESRANGE provides information on the dynamic state of the atmosphere, winds and waves. Whenever lidar measurements are possible, these are used to complement the in situ balloon-borne measurements. One lidar is located at IRF (about 30 km away from ESRANGE) and another one is

located at ESRANGE close to the balloon launch pad. The lidar at IRF (Voelger and Nikulin, 2005) is an elastic backscatter lidar and the one at ESRANGE is a Raman–Mie lidar (Blum and Fricke, 2005). When retrieving the extinction coefficients from lidar measurements, an uncertainty arises from the fact that the lidar ratio (extinction coefficient divided by backscatter coefficient) is not known. An additional uncertainty stems from the fact that the lidar beam and B-ICI do not sample the cloud at the same location. Even though air parcels sampled by the lidar may advect close to the balloon trajectory, a certain distance usually remains. Despite these uncertainties, a preliminary study found that the extinction coefficients retrieved from lidar measurements compare favourably with the extinction measurements of B-ICI (Kuhn et al., 2017). However, here we have not retrieved the extinction coefficient, and the remaining distance between lidar and B-ICI measurements has not been considered. In this study, only the backscattered signal is directly used as complementary information to assess the temporal and spatial characteristics of the ice clouds sampled with the B-ICI.

## 3 Classification of measurements

Data from eight measurement flights are presented in this study. The following subsections describe the classification of the clouds probed on those days. In Table 1 the flight times of the balloons and the classification of the cirrus clouds by weather conditions (see Sect. 3.1) and formation origin (see Sect. 3.2) are listed. In Sect. 3.3, the microphysical properties of the observed ice clouds are presented.

### 3.1 Weather conditions

Weather conditions on the measurement days have been analysed using weather maps, such as ground pressure with frontal analysis (from Deutscher Wetterdienst) and 500 hPa geopotential (from <http://www.wetter3.de>, last access: 22 November 2018), and IR satellite images (from MSG-EUMETSAT, <http://www.woksat.info/wos.html>, last



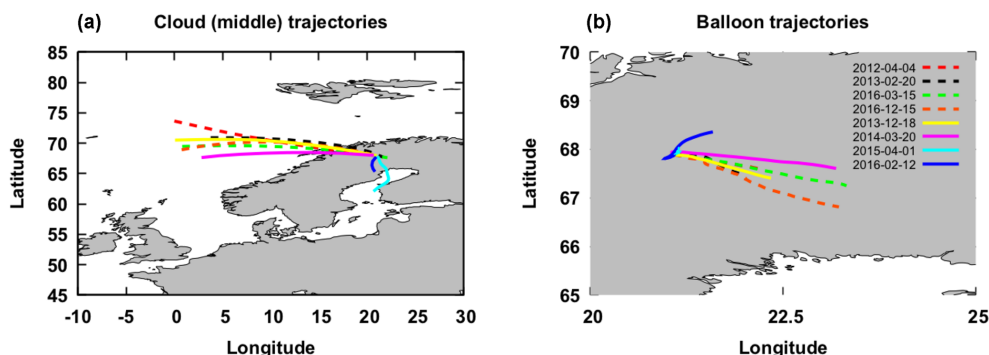


**Figure 3.** (a) The 24 h back trajectories of the average cloud height air mass for all days are shown and (b) the trajectories of the balloon measurements (dashed lines: in situ origin, solid lines: liquid origin). The air mass back trajectory latitudes and longitudes are calculated by CLaMS. The balloon coordinates were measured by the RS92 sonde.

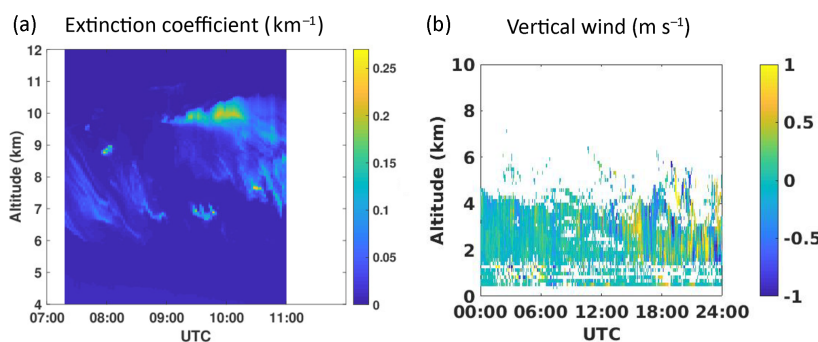


**Figure 4.** Extinction coefficient in  $\text{km}^{-1}$  derived from IRF lidar (a) and vertical velocity in  $\text{m s}^{-1}$  obtained from ESRAD on 20 February 2013 (b).

access: 22 November 2018). The wind direction is ascertained with the help of the balloon trajectories and the back trajectories of the air mass. Figure 3 shows the back trajectories of air parcels at middle cloud heights (arithmetic mean between the bottom and top of the cloud) for 24 h before the flight (Fig. 3a) and the trajectories of the in situ imager flights (Fig. 3b). It can be seen that the wind came from the south only on two of the eight days. On all other days, the wind direction was north-west and thus over the Scandinavian Mountains. In this case, waves can occur. Indications for this have been observed by ESRAD or lidar on four days. For one day (20 February 2013), Fig. 4 shows the lidar extinction coefficient (a) and the ESRAD vertical velocity (b). The radar can yield vertical velocities based on the Doppler shift of the backscatter signal. The variation in vertical velocities over time and altitude show very clearly that there were waves present at that time, and the horizontal wind direction points to the mountain range as source. In the case of lidar, the extinction coefficient shows the appearance and disappearance of clouds and the slope of clouds (inclination of cloud stripes on the altitude–time plot), which indicate waves.

The cirrus clouds were caused four times in the context of an occlusion and twice in relation to a warm front. Twice

the cirrus clouds were formed in front of a cold front due to strong wind and orographic uplift over the Scandinavian Mountains.

### 3.2 Cirrus origin

A simple and quite new method of classifying clouds is based on their origin. Two possible cirrus origins are distinguished, *liquid* and *in situ*. This classification is described in detail by Krämer et al. (2016) and Luebke et al. (2016) and is briefly outlined in the following.

The classification is based on cloud origin temperature, i.e. the temperature during formation of the cloud.

1. In situ origin cloud: homogeneous freezing of solution droplets or heterogeneous (deposition nucleation) at temperatures  $< 235 \text{ K}$  (with  $\text{RH}_{\text{water}} < 1$ , and  $\text{RH}_{\text{ice}} > 1$ ).
2. Liquid origin cloud: heterogeneous or homogeneous freezing of pre-existing cloud droplets at temperatures  $> 235 \text{ K}$  (with  $\text{RH}_{\text{water}} < \sim 1$  and  $\text{RH}_{\text{ice}} > 1$ ). In the case of a liquid origin cloud, the ice particles formed at lower altitudes via the liquid phase and were subsequently lifted to the cirrus temperature range ( $< 235 \text{ K}$ ).

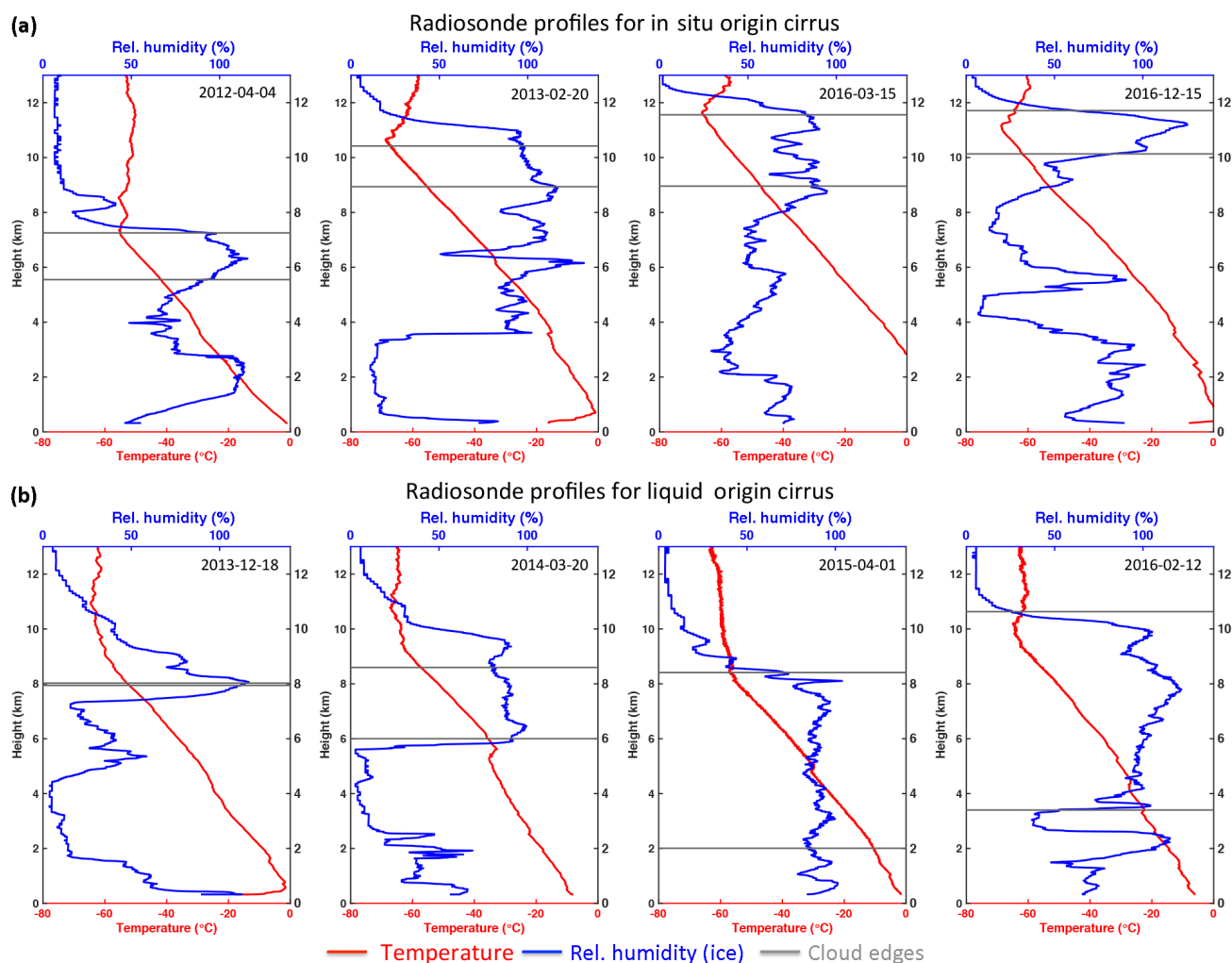


**Figure 5.** Temperature (red) and relative humidity profiles (blue) with respect to ice for the eight measurement days (**a**: in situ origin, **b**: liquid origin). The clouds upper and lower edges are marked by horizontal lines.

As formation in this context, we consider the time when the IWC started to be greater than zero, or 24 h before the in situ measurement in case IWC was greater than zero during these 24 h. Consequently, the cirrus origin is determined here using temperature and IWC along 24 h back trajectories. The Lagrangian microphysical model CLaMS-Ice (Luebke et al., 2016) is used to calculate these trajectories, starting from locations along the balloon flight paths, based on ECMWF ERA-Interim meteorological fields as input. Temperature is interpolated onto the trajectories, whereas the IWC along the trajectories is simulated with CLaMS-Ice. The origin of an observed cirrus cloud is identified as in situ origin if the temperature of the trajectory is always below 235 K. In case the temperature was originally higher than 235 K and the trajectory already carried IWC at the time temperature crossed 235 K towards colder values, the observed cirrus is assigned as liquid origin. The resulting classifica-

tions are listed in Table 1. Half of the measured cirrus clouds are classified as in situ origin, the other half as liquid origin.

### 3.3 Cloud properties

The cloud extent and average temperature for each measurement are listed in Table 1, and Fig. 5 shows the corresponding temperature and humidity profiles. Two cirrus clouds (1 April 2015 and 12 February 2016) have a vertical extension of approximately 6 km with a low cloud base at altitudes of 2 and 3 km, respectively. It may not be correct to call these clouds cirrus. However, in both cases, the entire cloud contains ice phase only, and the lower level represents, as will be discussed later, a glaciated and previously mixed-phase cloud layer. We believe these to be interesting cases and included them in our cirrus study. The other six cirrus clouds are thinner (80 m to 2 km thick) and had a higher cloud base (over 6 km). In all cases the temperature decreases with alti-

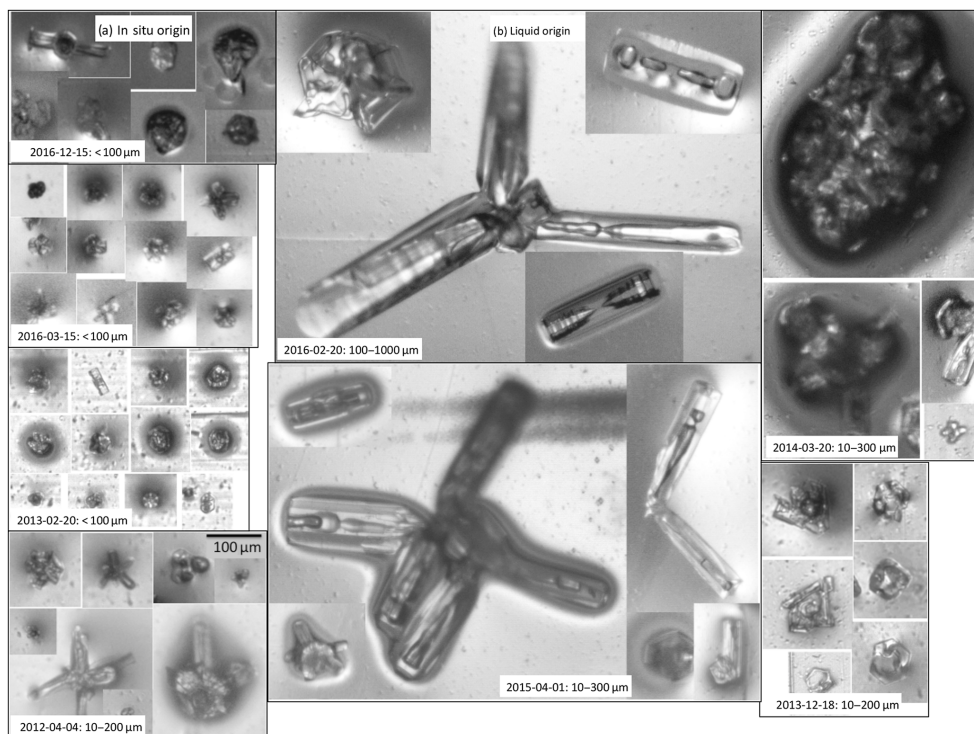


**Figure 6.** Some pictures of ice particles from all measurement days. The left panel shows ice particles from in situ origin cirrus, on the right liquid origin crystals are displayed. For a better understanding of the size, a 100  $\mu\text{m}$  bar is displayed (4 April 2012 bottom). All images have the same scale resolution and 100  $\mu\text{m}$  corresponds to 61 pixels.

tude. The temperature at the cloud tops is between  $-60$  and  $-70$   $^{\circ}\text{C}$ . At the cloud bases, the temperature is between  $-45$  and  $-55$   $^{\circ}\text{C}$  in the case of thin clouds and between  $-10$  and  $-20$   $^{\circ}\text{C}$  in the case of the two thick clouds. The relative humidity with respect to ice in the clouds is between 80 % and 130 %. Particles with sizes between 10 and 1200  $\mu\text{m}$  have been collected. Smaller particles are not efficiently sampled (Kuhn and Heymsfield, 2016), and larger particles have not been encountered. Table 2 lists the size ranges and mean number concentration for each cloud. The ice particle number concentrations are between  $3\text{ L}^{-1}$  and  $400\text{ L}^{-1}$  and the profiles of the number concentration for each measurement day are shown in Fig. 8. For each measured cirrus cloud, the frequency of occurrence of shapes is summarized in Table 2 as percentages corresponding to the five particle shape groups (compact, irregular, rosettes, plates and columnar). Some images of the particles from each measurement are shown in Fig. 6. All particle images are shown with the same size scaling.

## 4 Results and discussion

### 4.1 Size and number concentration

Our measurements show differences in particle size and number concentration depending on cloud origin. This dif-

ference in size is also reflected in the number size distribution (PSD). Figure 7 shows PSDs for all measurement cases, where possible also for different height levels. In cases of in situ origin cirrus, all particles are smaller than 350  $\mu\text{m}$ . On three of the four days with in situ origin (20 February 2013, 15 March 2016 and 15 December 2016) all particles are even smaller than 100  $\mu\text{m}$ . The in situ origin PSDs are fairly narrow, which indicates that the corresponding clouds were quite young, homogeneously formed cirrus, where the ice crystals have not yet grown to larger sizes. On 4 April 2012, the ice particles may have grown somewhat more than on the other days with in situ origin clouds, leading to somewhat wider PSDs on that day. All distributions of the liquid origin clouds extend to larger sizes and are broader than in the case of the in situ origin. In order for the particles to grow that large, a sufficiently high temperature with the related high water vapour concentration is required. Such conditions are given for liquid origin clouds. The PSDs of the two liquid origin clouds, originating from the south (1 April 2015 and 12 February 2016) with low cloud base (totally frozen, previously mixed-phase cloud) and large vertical extension, are particularly wide. On these two days (see Table 2 and Fig. 7) we have collected very large ice particles, with maximum sizes of approximately 600 and 1200  $\mu\text{m}$ , respectively. The other two liquid origin clouds have similarly narrow PSDs as the in situ origin clouds and have proba-



**Table 2.** List of days, mean number concentration  $n$ , mean particle  $D_{\max}$ , and relative number (in %) of particles in different shape groups.

Date – origin	$n$	$D_{\max}$	Compact	Irregulars	Rosettes	Plates	Columnar
	$\text{L}^{-1}$	min/median/max $\mu\text{m}$					
4 Apr 2012 – in situ	37	7/96/327	38.8	42.2	16.4	0.4	2.2
20 Feb 2013 – in situ	228	14/34/91	71.7	19.3	2.5	1.8	4.7
15 Mar 2016 – in situ	13	25/41/105	72.4	21.3	4.6	0.7	1.0
15 Dec 2016 – in situ	3	25/52/102	63.9	16.8	4.2	0.0	15.1
18 Dec 2013 – liquid	16	24/84/277	4.3	69.6	6.5	8.7	10.9
20 Mar 2014 – liquid	38	11/100/492	27.2	60.8	9.5	0.3	2.2
1 Apr 2015 – liquid	8	22/201/643	7.2	23.9	49.3	1.6	18.0
12 Feb 2016 – liquid	6	5/244/1228	6.0	39.2	28.5	3.7	22.6

bly been already in the process of dissolving, and large particles lost via precipitation. On 18 December 2013, for example, the cloud is very thin (80 m) and the relative humidity (ice) above and below the cloud is even strongly undersaturated. Many of the collected particles look as if parts have already sublimated. Data reported earlier from aircraft measurements at high latitudes also show a large range in sizes comparable to the observations of our balloon measurements. Gayet et al. (2007) described a measurement in which they collected falling ice particles from a cirrus cloud above. The size distribution between 25 and 1000  $\mu\text{m}$  mentioned by them corresponds well with our two thick liquid origin clouds, which had their lower edge approximately at the same height and similar temperature. Furthermore, Sourdeval et al. (2018) presented PSDs from five aircraft campaigns (tropics: ATTREX, ACRIDICON-CHUVA; midlatitudes: SPARTICUS, ML-CIRRUS and COALESC). In the averaged data, they observed, in addition to a primary mode of sub 100  $\mu\text{m}$  particles that was always present, a secondary mode of larger than 100  $\mu\text{m}$  particles that appeared only at temperatures higher than  $-50^\circ\text{C}$ . They discussed that this large particle mode was due to liquid origin cirrus. Thus, a comparison with our measurements shows that in the Arctic liquid origin clouds with larger particles can still occur at lower temperatures.

In general, the PSDs are more narrow and the number concentration ( $n$ ) higher with increasing height and decreasing temperature. This can be clearly seen, for example, for the in situ origin clouds in Figs. 7 and 8. The dependence of in situ origin PSDs and  $n$  on altitude and temperature is likely due to the main ice nucleation zone being at the cloud top. This dependence of the PSDs and  $n$  has also been found on a global scale (e.g. Sourdeval et al., 2018; Gryspeerd et al., 2018). This PSD and  $n$  trend with altitude and temperature is not clearly seen for the liquid origin cirrus cases. This could be explained by the fact that liquid origin cirrus form at lower altitudes and then ascent in the prevailing updraught. The few ice particles, nucleated in warmer and thus also moister air masses, grow to large sizes which sediment out of the air

mass while ascending. This means that in pure liquid origin cirrus there is no process enhancing the number concentration of smaller ice particles towards the cloud top or higher altitude.

However, these variations in PSDs with altitude or temperature are less than the general differences observed between in situ origin and liquid origin. The broadest size distribution at the lowest height of the in situ origin cloud on 20 February 2013, for example, is still much more narrow than any distribution of the liquid origin cloud on 12 February 2016. This is also true for the other measurement days, even when considering the two liquid origin clouds with narrower PSDs, which are still broader than in situ PSDs at similar temperatures. That means that size distributions measured in different clouds but at similar altitudes and temperatures can be significantly different. While these differences are obviously not only related to the local ambient conditions, they are strongly related to the cloud origin.

The total number concentrations are shown in Fig. 8 as altitude profiles for all eight measurement days (a: in situ origin, b: liquid origin). The number concentrations of the liquid origin clouds are relatively low (5 to 70  $\text{L}^{-1}$ ). The lower  $n$  in comparison to Luebke et al. (2016), who found a median ice number concentration slightly above 100  $\text{L}^{-1}$  in liquid origin midlatitude cirrus, might be due to a lower number of ice nucleating particles (INPs) in Arctic regions (Costa et al., 2017), which are necessary for heterogeneous freezing. However, low number concentrations could also be caused by a dissolving cloud state. To confirm this, one would need INP or humidity measurements during some time before our measurements, hence we can only speculate here.

Comparing 20 February 2013 and 12 February 2016, it can be seen that the maximum concentration of the in situ origin cloud is approximately 20 times greater than in the liquid origin cloud. This much higher number concentration in the case of this in situ origin cloud does not apply to all of our in situ origin cases, but only to two measurements (20 February 2013 and 4 April 2012). On 15 March 2016,  $n$  is similar as in the case of liquid origin measurements and on 15 De-

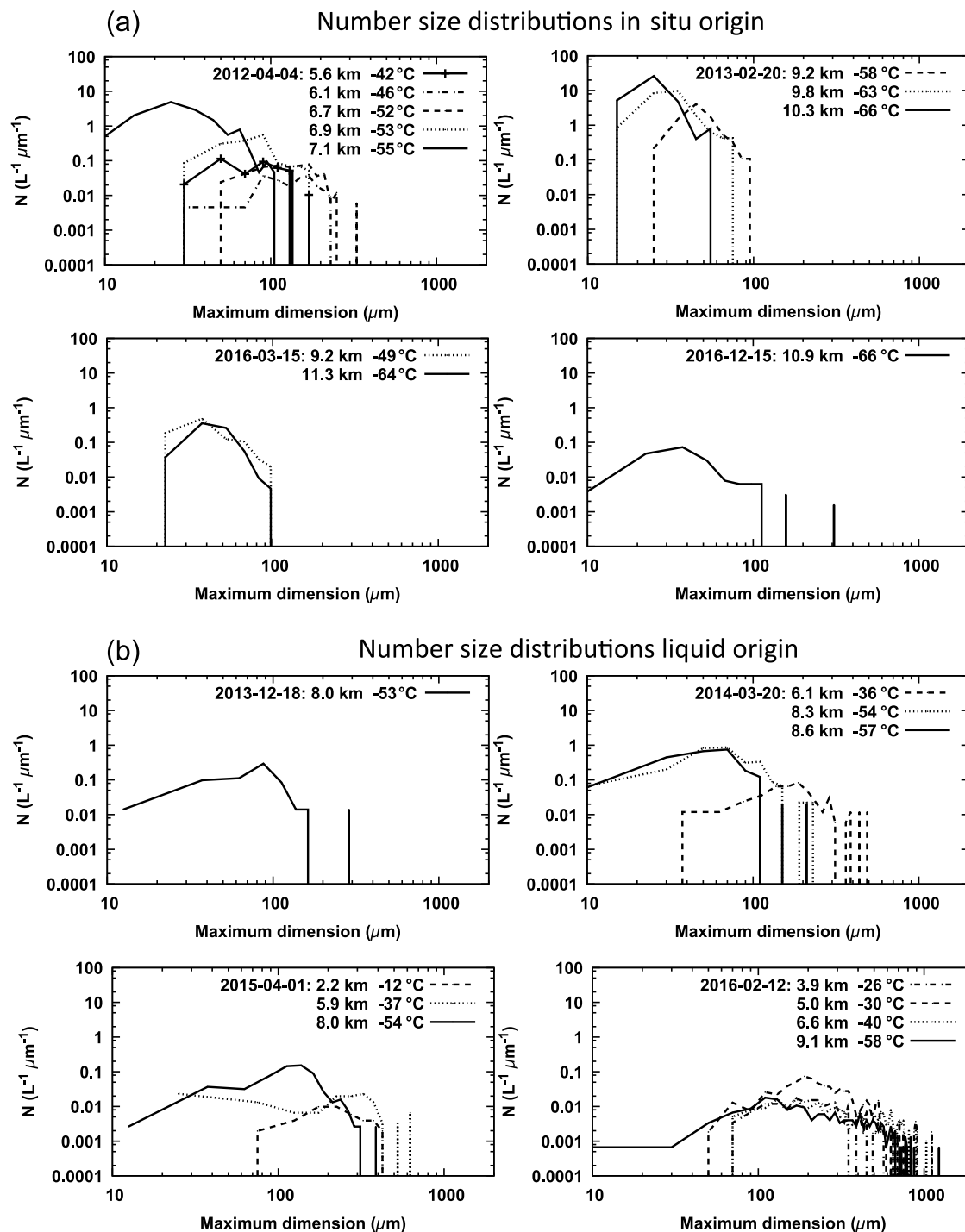


**Figure 7.** Number size distributions for all measurement days for different cloud levels (a: in situ origin; b: liquid origin).

cember 2016  $n$  is very low with just  $3 \text{ L}^{-1}$ . Such high differences in  $n$  between in situ origin clouds may be related to the influence of wave activity. The two days (20 February 2013 and 4 April 2012) with higher number concentration ( $300\text{--}400 \text{ L}^{-1}$ ) and also 15 March 2016 are connected to very strong winds coming from the north-west that have led

to waves, which have been observed by ESRAD or lidar on both days. These waves with their related high vertical velocities can be the needed trigger for such high number concentrations (e.g. Lohmann and Kärcher, 2002). Field et al. (2001) showed that number concentrations in wave clouds can even rise with decreasing temperature up to  $100\,000 \text{ L}^{-1}$ .

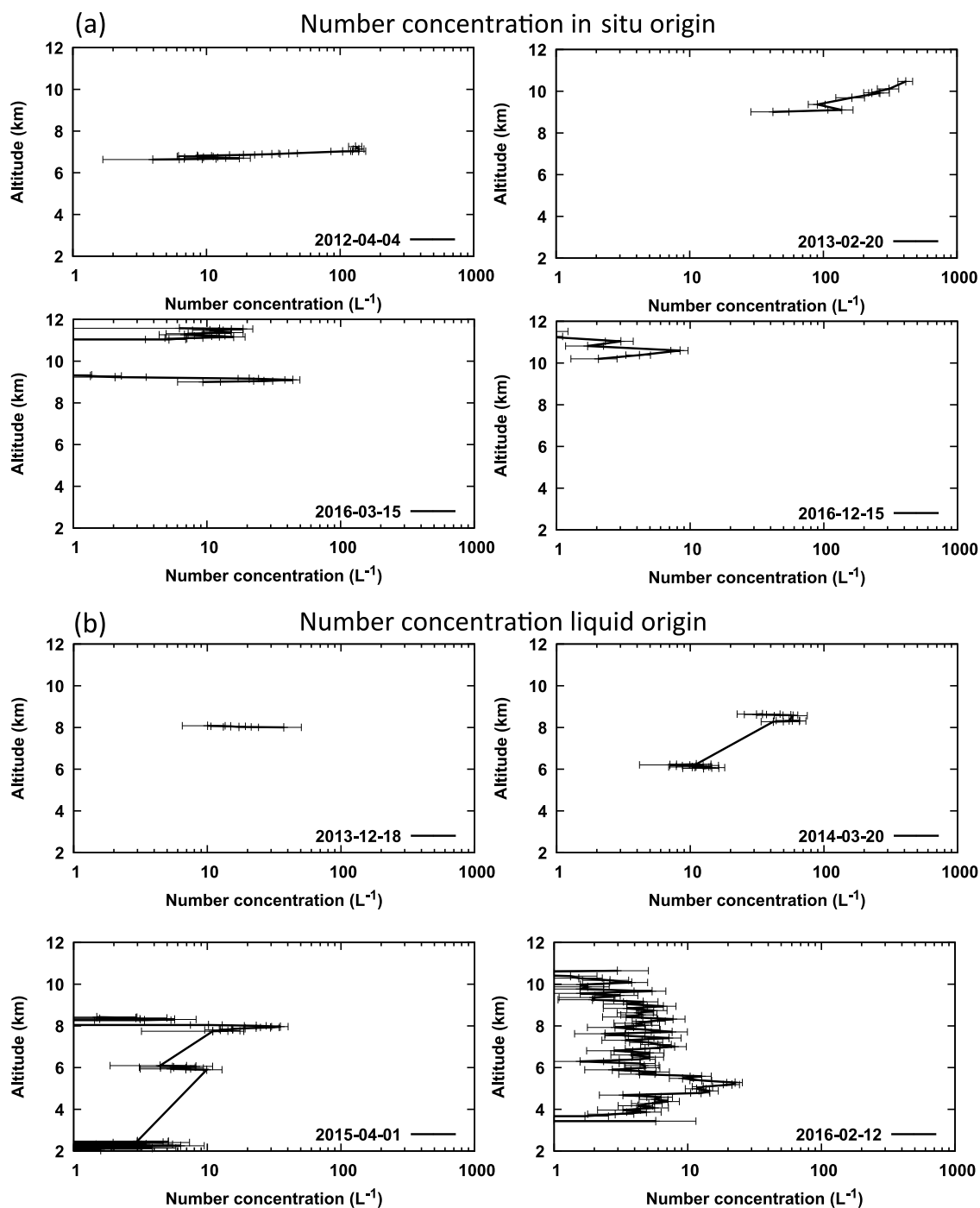


**Figure 8.** PSDs at different cloud levels for all measurement days (**a**: in situ origin; **b**: liquid origin).

In contrast, the midlatitude in situ origin cirrus observations, described by Krämer et al. (2016) and Luebke et al. (2016), showed lower  $n$  than those in the Arctic. The reason may be that most of the Arctic in situ observations are influenced by waves with high vertical velocities triggering homogeneous nucleation of many ice crystals. Such observa-

tions were very rare in Krämer et al. (2016) and Luebke et al. (2016).

Krämer et al. (2016) discussed two types of in situ origin cirrus. The first type appears in slow updraughts, e. g. in warm conveyor belts. The ice is nucleated mostly heterogeneously and the corresponding ice particle number concentrations are in the range of the available INPs and rather low.

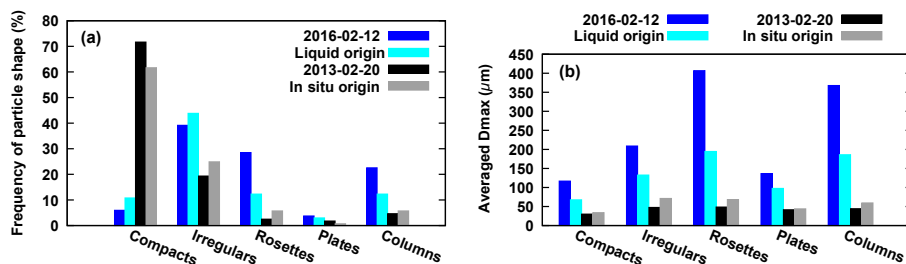


**Figure 9.** Occurrence of different particle shapes depending on cloud origin (a) and average  $D_{\max}$  for the different shapes (b). Mean values of shape and size of the four in situ origin (grey) measurements and four liquid origin (light blue) measurements. Mean values of shape and size of one in situ origin measurement day (black) and of one liquid origin measurement day (blue).

This applies to the majority of the measurements analysed by Krämer et al. (2016) and Luebke et al. (2016) and to one of our measurement days (15 December 2016).

In the second type which is related to fast updraughts, the ice particles formed by homogeneous nucleation. This is reflected in a high number concentration and is more often the case in our measurements. As a result, in our case three of the in situ origin clouds have higher or about the same  $n$  as liquid origin clouds.

Liquid origin clouds are typically present in the case of convection or large-scale transport such as warm conveyor belts. The cirrus ice particles of liquid origin are mostly formed by heterogeneous freezing at lower altitudes and temperatures above 235 K, where typically mixed-phase clouds occur. They are uplifted into the in situ temperature range where they at last fully glaciate. In the original altitude, more water vapour and INPs are available, resulting together with the continuous updraught in larger particles, higher number concentration and thus higher IWC compared to the in situ origin clouds with slow updraught. As indicated earlier, differences between midlatitudes and high latitudes may then be explained by differences in the available INPs for liquid origin clouds and the larger influence of waves on our measurement cases in the Arctic in the case of in situ origin.

## 4.2 Shape

In our individual cases there is no significant dependence of the shape on temperature and relative humidity (with respect to ice). Furthermore, no particular dependence of particle shape over the height was found. Therefore, we are reporting the average frequency of occurrence of the different particle shapes (see Table 2) and discuss how that varies depending on cloud origin. These average frequencies of shape occurrence for in situ origin and for liquid origin clouds are also shown in Fig. 9a. Figure 9b shows how the average particle sizes of the different shapes vary depending on the cloud origin. As can be seen in Figs. 6 and 9, in the case of in situ origin, the particles are usually small in size and compact or irregular in shape. However, in the case of liquid origin, the particles are most commonly irregular and rosettes.

In situ origin clouds form at a temperature range ( $< 235$  K) where the water concentration in the atmosphere is much lower than at the warmer temperatures at which ice forms in liquid origin clouds. This, combined with the usually higher number concentrations of ice particles formed in in situ origin clouds (fast updraughts) and the resulting competition for water vapour, does not allow for forming very large and complex particles. Hence, it is understandable that most of the in situ origin cirrus particles found were compact. It should be noted that in some cases large ice crystals can also form in in situ origin clouds under calm (low vertical updraughts) or clean conditions (low INP concentration). In these cases, the number concentration would be very low, which in turn would allow the ice crystals to grow to larger sizes (e.g. Jensen et al., 2008). However, this type of cirrus cloud is not dominating our observations or the large collection by Krämer et al. (2016) and Luebke et al. (2016).

While compact particles are on average the smallest ones, rosettes, irregular and columnar particles in liquid origin clouds are largest. Liquid origin cirrus clouds, in contrast to in situ origin cirrus, form at warmer temperatures with higher water vapour content in the air. Therefore, the ice particles can grow larger and also to more complex shapes. Particularly large ice particles have been observed on the two days (1 April 2015 and 12 February 2016) where the lower part of the cloud was in the temperature regime of mixed-phase clouds. As discussed earlier, at the time of measurement these two clouds were completely frozen. However, the liquid water, which was probably present at some earlier stage, has contributed to the observed extensive growth. This is in agreement with Bailey and Hallett (2009), who claimed that a high supersaturation is needed for the growth of rosettes and hollow columns, which are abundant on those days. Fewer rosettes are found on the other two days (18 December 2013 and 20 March 2014). This may be unexpected; however, it may be explained by larger particles falling out of the probably ageing clouds. In fact, these clouds look like they have been in the process of dissolving, as discussed earlier in Sect. 4.1.

It is noticeable that almost all columnar particles and rosettes are hollow in the case of liquid origin cirrus. This

corroborates findings by others (e.g. Weickmann, 1949; Heymsfield et al., 2002; Schmitt et al., 2006) in which measurements showed that around 80 % of all collected rosettes were hollow to a certain extent. In the case of in situ origin cirrus there are very few, and if present, then very small rosettes and columns. Thus, a statement regarding their hollowness would be rather speculative.

The supersaturation present in our liquid origin cloud measurements is most of the time too low to directly explain growth of our observed hollow rosettes and columns. According to laboratory measurements by Bailey and Hallett (2004), existence of hollow rosettes requires high supersaturation, and hollowness of rosettes is more likely at higher temperatures ( $> -40^{\circ}\text{C}$ ). While the temperature and water vapour at which the particles have been detected is too low, ambient properties at the origin of the clouds met the conditions for hollow rosette growth in the case of liquid origin clouds. Thus, this demonstrates once more that environmental conditions at cloud origin are crucial for explaining observations.

In both origin cases, plates and columnar particles have been rarely collected. They are on average less frequent than any of the other shapes. This is similar to Korolev et al. (1999) who collected only 3 % of these shapes. In Table 2 it can be seen that in the case of in situ origin clouds on 20 February 2013 the highest percentage of plates has been sampled with only 1.8 %. Somewhat more columns have been collected, on average 5.7 %. In the case of liquid origin these particle shapes are on average more frequent than in the case of in situ origin, as can be seen in Fig. 9. Plates are on average 3.0 % of all observed ice particles, and columns are with 12.3 % even a little more frequent than compact particles (10.8 %).

Shape detection is sometimes intricate, even with high image resolution. Some particle shapes may be confusing, as also observed by others (e.g. Lindqvist et al., 2012). Here, the assignment between irregulars and rosettes is sometimes ambiguous, because in a few cases rosettes appear somewhat irregular. For example, some rosettes look as if they have a part missing or one bullet seems to be a longer column. In such cases, we have assigned these irregular rosettes to the shape group rosettes rather than to irregulars. In other cases, small compact ice particles sometimes show characteristics that indicate an initial formation of rosettes; however, we have still classified them as compact due to their spheroidal shape. Classifying them as rosettes would not have changed any of the results discussed here.

For ice particles smaller than  $20\text{ }\mu\text{m}$  the shape is difficult to recognize and, consequently, some misclassification may occur leading to over-representation of compact in this size range and under-representation of other shapes such as plates and rosettes. However, on the day with the smallest particles (20 February 2013) only about 6 % of all particles are smaller than  $20\text{ }\mu\text{m}$ . Thus, this issue of potential misclassification will likely not alter our findings significantly.

## 5 Summary and conclusions

In this study, eight balloon-borne in situ measurements of Arctic cirrus clouds were analysed. The balloons were launched from Kiruna, Sweden, during winter time. Particular emphasis was placed on the analysis of ice particle size, shape and number concentration with respect to cirrus origin. Since in situ origin clouds are formed from the gas phase at temperatures below 235 K, while liquid origin clouds formed via liquid drops at temperatures above 235 K, the cloud and particle properties are expected to vary in accordance to cloud origin. Indeed, while large differences in particle size, shape and number concentration are observed between the various measurements, some similarities are noticed within the two groups of data with liquid and in situ origin clouds. These similarities and the differences between data, when grouped into liquid and in situ origin, are summarized below.

1. Particle size: Arctic cirrus clouds with particle sizes between 10 and  $1200\text{ }\mu\text{m}$  have been observed. Most common in our clouds are particles with sizes between 30 and  $250\text{ }\mu\text{m}$ . While in situ origin clouds have smaller particles with sizes below  $350\text{ }\mu\text{m}$ , liquid origin clouds exhibit larger particles and wider PSDs. The ice particles of clouds with wind from the south are much larger and fewer than ice particles from the west where the cirrus clouds were probably triggered by strong updraughts associated with waves behind the Scandinavian Mountains.
2. Particle shape: the in situ origin clouds consist mainly of compact and irregular particles and the liquid origin clouds of irregular, rosettes and columns. In both cases, there are hardly any plates. The compact particles are the smallest particles and rosettes are the largest. Rosettes and columns are mostly hollow.
3. Particle number: the measured number concentrations are between 3 and  $400\text{ L}^{-1}$ . Both extreme values have been determined for in situ origin clouds. The maximum concentrations have occurred due to waves on the lee side of the Scandinavian Mountains. In comparison, in previous campaigns in the midlatitudes lower number concentrations were measured for this cloud type. This may be explained by the fact that hardly any wave-induced in situ origin clouds were observed in these campaigns. Concentrations for liquid origin clouds are low (5 to  $70\text{ L}^{-1}$ ). In contrast, high number concentrations were measured in the midlatitudes for this cloud type, maybe caused by a higher number of INPs in the midlatitudes than in the Arctic.

The results of this study imply that remote-sensing retrievals and weather and climate models could be improved when accounting for these differences rather than using parameterizations that only depend on local conditions. Future work



will include more measurements for further significant statistical evaluation. In addition, we also want to allow several B-ICIs to fly one after the other in order to investigate a temporal development of the particle properties. Also, the in situ data may help to constrain the lidar ratio, which will be tested in future with more joint lidar and B-ICI data from our ongoing campaign.

*Data availability.* The presented data are available upon request.

*Author contributions.* TK designed the experimental study, VW and TK performed the B-ICI measurements and PV the Lidar measurements, VW and TK did the image analysis, VW did the shape classification, VW and PV did the wave analysis, MK and CR performed the CLaMS Model calculation, MK, CR and VW analysed cirrus origin, VW and MM performed the weather analysis, VW wrote the manuscript with contribution from all other authors.

*Competing interests.* The authors declare that they have no conflict of interest.

*Acknowledgements.* We thank Peter Dalin (IRF) and Evgenia Belova (IRF) for interpreting and discussing the ESRAD data in terms of gravity and mountain lee waves. We thank the Swedish National Space Agency for funding these balloon campaigns (grants Dnr 85/10, Dnr 86/11, Dnr 143/12, Dnr 273/12, Dnr 168/13, Dnr 124/14), and the Graduate School of Space Technology at Luleå University of Technology for additional financial support.

Edited by: Timothy Garrett

Reviewed by: two anonymous referees

## References

- Bailey, M. and Hallett, J.: Growth Rates and Habits of Ice Crystals between  $-20^{\circ}$  to  $-70^{\circ}\text{C}$ , *J. Atmos. Sci.*, 61, 514–544, [https://doi.org/10.1175/1520-0469\(2004\)061<0514:GRAHOI>2.0.CO;2](https://doi.org/10.1175/1520-0469(2004)061<0514:GRAHOI>2.0.CO;2), 2004.
- Bailey, M. P. and Hallett, J.: A comprehensive habit diagram for atmospheric ice crystals: Confirmation from the laboratory, AIRS II, and other field studies, *J. Atmos. Sci.*, 66, 2888–2899, <https://doi.org/10.1175/2009JAS2883.1>, 2009.
- Baumgardner, D., Abel, S. J., Axisa, D., Cotton, R., Crosier, J., Field, P., Gurganus, C., Heymsfield, A., Korolev, A., Krämer, M., Lawson, P., McFarquhar, G., Ulanowski, Z., and Um, J.: Cloud Ice Properties: In Situ Measurement Challenges, *Meteor. Mon.*, 58, 9.1–9.23, <https://doi.org/10.1175/AMSMONOGRAPH-D-16-0011.1>, 2017.
- Blum, U. and Fricke, K. H.: The Bonn University lidar at the Esrange: technical description and capabilities for atmospheric research, *Ann. Geophys.*, 23, 1645–1658, <https://doi.org/10.5194/angeo-23-1645-2005>, 2005.
- Boucher, O., Randall, D., Artaxo, P., Bretherton, C., Feingold, G., Forster, P., Kerminen, V.-M., Kondo, Y., Liao, H., Lohmann, U., Rasch, P., Satheesh, S., Sherwood, S., Stevens, B., and Zhang, X.: Clouds and Aerosols. In: *Climate Change 2013: The Physical Science Basis. Contribution of Working Group I to the Fifth Assessment Report of the Intergovernmental Panel on Climate Change*, edited by: Stocker, T. F., Qin, D., Plattner, G.-K., Tignor, M., Allen, S. K., Boschung, J., Nauels, A., Xia, Y., Bex, V., and Midgley, P. M., Cambridge University Press, Cambridge, United Kingdom and New York, NY, USA, 2013.
- Costa, A., Meyer, J., Afchine, A., Luebke, A., Günther, G., Dorsey, J. R., Gallagher, M. W., Ehrlich, A., Wendisch, M., Baumgardner, D., Wex, H., and Krämer, M.: Classification of Arctic, midlatitude and tropical clouds in the mixed-phase temperature regime, *Atmos. Chem. Phys.*, 17, 12219–12238, <https://doi.org/10.5194/acp-17-12219-2017>, 2017.
- Field, P. R., Cotton, R. J., Noone, K., Glantz, P., Kaye, P. H., Hirst, E., Greenaway, R. S., Jost, C., Gabriel, R., Reiner, T., Andreae, M., Saunders, C. P. R., Archer, A., Choularton, T., Smith, M., Brooks, B., Hoell, C., Bandy, B., Johnson, D., and Heymsfield, A.: Ice nucleation in orographic wave clouds: Measurements made during INTACC, *Q. J. Roy. Meteor. Soc.*, 127, 1493–1512, <https://doi.org/10.1256/smsqj.57501>, 2001.
- Freeman, K. P. and Liou, K.: Climatic effects of cirrus clouds, *Adv. Geophys.*, 21, 231–288, 1979.
- Gayet, J.-F., Stachlewska, I. S., Jourdan, O., Shcherbakov, V., Schwarzenboeck, A., and Neuber, R.: Microphysical and optical properties of precipitating drizzle and ice particles obtained from alternated lidar and in situ measurements, *Ann. Geophys.*, 25, 1487–1497, <https://doi.org/10.5194/angeo-25-1487-2007>, 2007.
- Gryspeerd, E., Sourdeval, O., Quaas, J., Delanoë, J., Krämer, M., and Kühne, P.: Ice crystal number concentration estimates from lidar-radar satellite remote sensing – Part 2: Controls on the ice crystal number concentration, *Atmos. Chem. Phys.*, 18, 14351–14370, <https://doi.org/10.5194/acp-18-14351-2018>, 2018.
- Gu, Y., Liou, K. N., Ou, S. C., and Fovell, R.: Cirrus cloud simulations using WRF with improved radiation parameterization and increased vertical resolution, *J. Geophys. Res.*, 116, D06119, <https://doi.org/10.1029/2010JD014574>, 2011.
- Heymsfield, A. J., Lewis, S., Bansemer, A., Iaquinta, J., Miloshevich, L. M., Kajikawa, M., Twohy, C., and Poellot, M. R.: A General Approach for Deriving the Properties of Cirrus and Stratiform Ice Cloud Particles, *J. Atmos. Sci.*, 59, 3–29, [https://doi.org/10.1175/1520-0469\(2002\)059<0003:AGAFDT>2.0.CO;2](https://doi.org/10.1175/1520-0469(2002)059<0003:AGAFDT>2.0.CO;2), 2002.
- Heymsfield, A., Krämer, M., Luebke, A., Brown, P., Czicz, D. J., Franklin, C., Lawson, P., Lohmann, U., McFarquhar, G., Ulanowski, Z., and Van Tricht, K.: Cirrus Clouds, *Meteor. Mon.*, 58, 2.1–2.26, <https://doi.org/10.1175/AMSMONOGRAPH-D-16-0010.1>, 2017.
- Jackson, R. C., McFarquhar, G. M., Stith, J., Beals, M., Shaw, R. A., Jensen, J., Fugal, J., and Korolev, A.: An assessment of the impact of antishattering tips and artifact removal techniques on cloud ice size distributions measured by the 2-D cloud probe, *J. Atmos. Ocea. Tech.*, 31, 2567–2590, <https://doi.org/10.1175/JTECH-D-13-00239.1>, 2014.
- Jensen, E. J., Pfister, L., Bui, T. V., Lawson, P., Baker, B., Mo, Q., Baumgardner, D., Weinstock, E. M., Smith, J. B., Moyer, E. J., Hanisco, T. F., Sayres, D. S., Clair, J. M. St., Alexander, M. J.,

- Toon, O. B., and Smith, J. A.: Formation of large ( $\approx 100\mu\text{m}$ ) ice crystals near the tropical tropopause, *Atmos. Chem. Phys.*, 8, 1621–1633, <https://doi.org/10.5194/acp-8-1621-2008>, 2008.
- Kienast-Sjögren, E., Rolf, C., Seifert, P., Krieger, U. K., Luo, B. P., Krämer, M., and Peter, T.: Climatological and radiative properties of midlatitude cirrus clouds derived by automatic evaluation of lidar measurements, *Atmos. Chem. Phys.*, 16, 7605–7621, <https://doi.org/10.5194/acp-16-7605-2016>, 2016.
- Kirkwood, S., Wolf, I., Nilsson, H., Dalin, P., Mikhaylova, D., and Belova, E.: Polar mesosphere summer echoes at Wasa, Antarctica ( $73^\circ\text{S}$ ): First observations and comparison with  $68^\circ\text{N}$ , *Geophys. Res. Lett.*, 34, L15803, <https://doi.org/10.1029/2007GL030516>, 2007.
- Knollenberg, R. G.: Techniques for probing cloud microstructure, in: *Clouds, Their Formation, Optical Properties and Effects*, edited by: Hobbs, P. V. and Deepack, A., Academic Press, New York, 15–91, 1981.
- Korolev, A., Emery, E., and Creelman, K.: Modification and tests of particle probe tips to mitigate effects of ice shattering, *Journal of Atmospheric and Oceanic Technology*, 30, 690–708, <https://doi.org/10.1175/JTECH-D-12-00047.1>, 2013.
- Korolev, A. V., Isaac, G. A., and Hallett, J.: Ice particle habits in Arctic clouds, *Geophys. Res. Lett.*, 26, 1299–1302, 1999.
- Korolev, A. V., Emery, E. F., Strapp, J. W., Cober, S. G., Isaac, G. A., Wasey, M., and Marcotte, D.: Small ice particles in tropospheric clouds: Fact or artifact? Airborne icing instrumentation evaluation experiment, *Bulletin of the American Meteorological Society*, 92, 967–973, <https://doi.org/10.1175/2010BAMS3141.1>, 2011.
- Krämer, M., Rolf, C., Luebke, A., Afchine, A., Spelten, N., Costa, A., Meyer, J., Zöger, M., Smith, J., Herman, R. L., Buchholz, B., Ebert, V., Baumgardner, D., Borrmann, S., Klingebiel, M., and Avallone, L.: A microphysics guide to cirrus clouds – Part I: Cirrus types, *Atmos. Chem. Phys.*, 16, 3463–3483, <https://doi.org/10.5194/acp-16-3463-2016>, 2016.
- Kuhn, T. and Heymsfield, A. J.: In Situ Balloon-Borne Ice Particle Imaging in High-Latitude Cirrus, *Pure Appl. Geophys.*, 173, 3065–3084, <https://doi.org/10.1007/s00024-016-1324-x>, 2016.
- Kuhn, T., Grishin, I., and Sloan, J. J.: Improved Imaging and Image Analysis System for Application to Measurement of Small Ice Crystals, *J. Atmos. Ocean. Tech.*, 29, 1811–1824, 2012.
- Kuhn, T., Heymsfield, A. J., and Buehler, S. A.: Balloon-borne measurements of ice particle shape and ice water content in the upper troposphere over Northern Sweden, European Space Agency, ESA, 721 SP, 93–97, 2013.
- Kuhn, T., Wolf, V., Völger, P., Stanev, M., and Gumbel, J.: Comparison of in-situ balloon-borne and lidar measurement of cirrus clouds, in: *23rd ESA Symposium on European Rocket and Balloon Programmes and Related Research*, Visby, Sweden, 11–15 June 2017, [http://pac.spaceflight.esa.int/docs/23\\_PACSymposium.zip](http://pac.spaceflight.esa.int/docs/23_PACSymposium.zip), 2017.
- Lawson, P., O'Connor, D., Zmarzly, P., Weaver, K., Baker, B., Mo, Q., and Jonsson, H.: The 2DS (Stereo) Probe: Design and preliminary tests of a new airborne, high speed, high-resolution particle imaging probe, *J. Atmos. Ocean. Tech.*, 23, 1462–1477, 2006.
- Lawson, R. P., Baker, B. A., Schmitt, C. G., and Jensen, T. L.: An overview of microphysical properties of Arctic clouds observed in May and July 1998 during FIRE ACE, *J. Geophys. Res.*, 106, 14989–15014, 2001.
- Lindqvist, H., Muinonen, K., Nousiainen, T., Um, J., McFarquhar, G. M., Haapanala, P., Makkonen, R., and Hakkarainen, H.: Ice-cloud particle habit classification using principal components, *J. Geophys. Res.*, 117, D16206, <https://doi.org/10.1029/2012JD017573>, 2012.
- Liou, K.: Influence of cirrus clouds on weather and climate processes: a global perspective, *Mon. Weather Rev.*, 114, 1167–1199, 1986.
- Lohmann, U. and Kärcher, B.: First interactive simulations of cirrus clouds formed by homogeneous freezing in the ECHAM general circulation model, *J. Geophys. Res.*, 107, AAC 8–1–AAC 8–13, <https://doi.org/10.1029/2001JD000767>, 2002.
- Luebke, A. E., Afchine, A., Costa, A., Grooß, J.-U., Meyer, J., Rolf, C., Spelten, N., Avallone, L. M., Baumgardner, D., and Krämer, M.: The origin of midlatitude ice clouds and the resulting influence on their microphysical properties, *Atmos. Chem. Phys.*, 16, 5793–5809, <https://doi.org/10.5194/acp-16-5793-2016>, 2016.
- Lynch, D. K.: Cirrus, edited by: Lynch, D. K., Sassen, K., O'C. Starr, D., and Stephens, G., Oxford University Press, Cambridge, New York, 2002.
- McFarquhar, G. M., Ghan, S., Verlinde, J., Korolev, A., Strapp, J. W., Schmid, B., Tomlinson, J. M., Wolde, M., Brooks, S. D., Cziczo, D., Dubey, M. K., Fan, J., Flynn, C., Gultepe, I., Hubbe, J., Gilles, M. K., Laskin, A., Lawson, P., Leaitch, W. R., Liu, P., Liu, X., Lubin, D., Mazzoleni, C., MacDonald, A. M., Moffet, R. C., Morrison, H., Ovchinnikov, M., Shupe, M. D., Turner, D. D., Xie, S., Zelenyuk, A., Bae, K., Freer, M., and Glen, A.: Indirect and semi-direct aerosol campaign: The impact of arctic aerosols on clouds, *B. Am. Meteorol. Soc.*, 92, 183–201, <https://doi.org/10.1175/2010BAMS2935.1>, 2011.
- Platt, C. M. R.: The role of cloud microphysics in high-cloud feedback effects on climate change, *Nature*, 341, 428–429, 1989.
- Potter, G. L. and Cess, R. D.: Testing the impact of clouds on the radiation budgets of 19 atmospheric general circulation models, *J. Geophys. Res.*, 109, D02106, <https://doi.org/10.1029/2003JD004018>, 2004.
- Sassen, K. and Comstock, J. M.: A midlatitude cirrus cloud climatology from the facility for atmospheric remote sensing. Part III: Radiative properties, *J. Atmos. Sci.*, 58, 2113–2127, [https://doi.org/10.1175/1520-0469\(2001\)058<2113:AMCCCC>2.0.CO;2](https://doi.org/10.1175/1520-0469(2001)058<2113:AMCCCC>2.0.CO;2), 2001.
- Schiller, C., Afchine, A., Eicke, N., Feigl, C., Fischer, H., Giez, A., Konopka, P., Schlager, H., Tuitjer, F., Wienhold, F. G., and Zoeger, M.: Ice particle formation and sedimentation in the tropopause region: A case study based on in situ measurements of total water during POLSTAR 1997, *Geophys. Res. Lett.*, 26, 2219–2222, 1999.
- Schlimme, I., Macke, A., and Reichardt, J.: The impact of ice crystal shapes, size distributions, and spatial structures of cirrus clouds on solar radiative fluxes, *J. Atmos. Sci.*, 62, 2274–2283, <https://doi.org/10.1175/JAS3459.1>, 2005.
- Schmitt, C. G., Jaquinta, J., and Heymsfield, A. J.: The Asymmetry Parameter of Cirrus Clouds Composed of Hollow Bullet Rosette-Shaped Ice Crystals from Ray-Tracing Calculations, *J. Appl. Meteorol. Clim.*, 45, 973–981, <https://doi.org/10.1175/JAM2384.1>, 2006.
- Solomon, S., Qin, D., M., Manning, M., Chen, Z., Marquis, M., Averyt, K. B., Tignor, M., and Miller, H. L.: Climate change 2007: the physical science basis: Contribution of Working Group I to

- the Fourth Assessment Report of the Intergovernmental Panel on Climate Change, Cambridge University Press, Cambridge, New York, 996 pp., 2007.
- Sourdeval, O., Gryspeerdt, E., Krämer, M., Goren, T., Delanoë, J., Afchine, A., Hemmer, F., and Quaas, J.: Ice crystal number concentration estimates from lidar-radar satellite remote sensing – Part 1: Method and evaluation, *Atmos. Chem. Phys.*, 18, 14327–14350, <https://doi.org/10.5194/acp-18-14327-2018>, 2018.
- Spichtinger, P., Gierens, K., and Dörnbrack, A.: Formation of ice supersaturation by mesoscale gravity waves, *Atmos. Chem. Phys.*, 5, 1243–1255, <https://doi.org/10.5194/acp-5-1243-2005>, 2005.
- Tang, G., Panetta, R. L., Yang, P., Kattawar, G. W., and Zhai, P. W.: Effects of ice crystal surface roughness and air bubble inclusions on cirrus cloud radiative properties from remote sensing perspective, *J. Quant. Spectrosc. Ra.*, 195, 119–131, <https://doi.org/10.1016/j.jqsrt.2017.01.016>, 2017.
- Verlinde, J., Harrington, J. Y., McFarquhar, G. M., Yannuzzi, V. T., Avramov, A., Greenberg, S., Johnson, N., Zhang, G., Poellot, M. R., Mather, J. H., Turner, D. D., Eloranta, E. W., Zak, B. D., Prenni, A. J., Daniel, J. S., Kok, G. L., Tobin, D. C., Holz, R., Sassen, K., Spangenberg, D., Minnis, P., Tooman, T. P., Ivey, M. D., Richardson, S. J., Bahrman, C. P., Shupe, M., DeMott, P. J., Heymsfield, A. J., and Schofield, R.: The mixed-phase arctic cloud experiment, *B. Am. Meteorol. Soc.*, 88, 205–221, <https://doi.org/10.1175/BAMS-88-2-205>, 2007.
- Voelger, P. and Nikulin, G.: The new lidar system at the Swedish Institute of Space Physics in Kiruna: description and first measurements, *ESA-SP 590*, 590, 321–325, 2005.
- Weickmann, H. K.: Die Eisphase in der Atmosphäre, in: *Berichte des Deutschen Wetterdienstes in der US-Zone*, Bad Kissingen, 1949.
- Weigel, R., Spichtinger, P., Mahnke, C., Klingebiel, M., Afchine, A., Petzold, A., Krämer, M., Costa, A., Molleker, S., Reutter, P., Szakáll, M., Port, M., Grulich, L., Jurkat, T., Minikin, A., and Borrmann, S.: Thermodynamic correction of particle concentrations measured by underwing probes on fast-flying aircraft, *Atmos. Meas. Tech.*, 9, 5135–5162, <https://doi.org/10.5194/amt-9-5135-2016>, 2016.
- Wernli, H., Boettcher, M., Joos, H., Miltenberger, A. K., and Spichtinger, P.: A trajectory-based classification of ERA-Interim ice clouds in the region of the North Atlantic storm track, *Geophys. Res. Lett.*, 43, 6657–6664, <https://doi.org/10.1002/2016GL068922>, 2016.
- Wu, W. and McFarquhar, G. M.: On the Impacts of Different Definitions of Maximum Dimension for Nonspherical Particles Recorded by 2D Imaging Probes, *J. Atmos. Ocean. Tech.*, 33, 1057–1072, 2016.